Published in final edited form as:
FEBS J. 2012 May ; 279(9): 1621–1631. doi:10.1111/j.1742-4658.2011.08412.x.

Structural comparison of cytochromes P450 2A6, 2A13, and 2E1 with pilocarpine†

Natasha M. DeVore[1], **Kathleen M. Meneely**[1,#], **Aaron G. Bart**[1], **Eva S. Stephens**[1], **Kevin P. Battaile**[2], and **Emily E. Scott**[1,*]

[1]Department of Medicinal Chemistry, The University of Kansas, Lawrence, KS 66045

[2]Hauptman-Woodward Medical Research Institute, IMCA-CAT, 9700 S. Cass Ave., Bldg 435, Argonne, IL 60439

Summary

Human xenobiotic-metabolizing cytochrome P450 (P450) enzymes can each bind and monooxygenate a diverse set of substrates, including drugs, often producing a variety of metabolites. Additionally a single ligand can interact with multiple cytochrome P450 enzymes, but often the protein structural similarities and differences that mediate such overlapping selectivity are not well understood. Even though the P450 superfamily has a highly canonical global protein fold, there are large variations in the active site size, topology, and conformational flexibility. We have determined how a related set of three human cytochrome P450 enzymes bind and interact with a common inhibitor, the muscarinic receptor agonist drug pilocarpine. Pilocarpine binds and inhibits the hepatic CYP2A6 and respiratory CYP2A13 enzymes much more efficiently than the hepatic CYP2E1 enzyme. To elucidate key amino acids involved in pilocarpine binding, crystal structures of CYP2A6 (2.4 Å), CYP2A13 (3.0 Å), CYP2E1 (2.35 Å), and a CYP2A6 mutant enzyme, CYP2A6 I208S/I300F/G301A/S369G (2.1 Å), have been determined with pilocarpine in the active site. In all four structures, pilocarpine coordinates to the heme iron, but comparisons reveal how individual amino acids lining the active sites of these three distinct human enzymes interact differently with the inhibitor pilocarpine.

Hyperlinking to databases—The atomic coordinates and structure factors have been deposited in the Protein Data Bank, Research Collaboratory for Structural Bioinformatics, Rutgers University, New Brunswick, NJ (http://www.rcsb.org/) with the following codes: CYP2A6 with pilocarpine (**3T3R**), CYP2A6 I208S/I300F/G301A/S369G with pilocarpine (**3T3Q**), CYP2A13 with pilocarpine (**3T3S**), and CYP2E1 with pilocarpine (**3T3Z**).

Keywords

Cytochrome P450; CYP2A13; CYP2A6; CYP2E1; pilocarpine

*Corresponding Author: To whom correspondence should be addressed: The University of Kansas, 1251 Wescoe Hall Dr., Lawrence, KS 66045. Telephone: (785) 864-5559. Fax: (785) 864-5326. eescott@ku.edu.
#Present address, Department of Molecular Biosciences, The University of Kansas, 1200 Sunnyside Avenue, Lawrence, KS, 66045.

Author Contributions: NMD expressed, purified, and crystallized the CYP2A proteins, performed X-ray diffraction experiments, solved, and refined the CYP2A structures under the supervision of EES. AGB assisted with CYP2A13 refinement. KMM expressed, purified, and crystallized CYP2E1. KPB collected and processed the CYP2E1 X-ray data. The CYP2E1 structure was solved by EES and refined by KMM and NMD. NMD performed ligand binding titrations, while NMD, ESS, and AGB performed the inhibition studies. NMD and EES wrote the manuscript. All authors have edited and given approval to the final version of the manuscript.

Structural data are available in the Protein Data Bank database under the accession numbers **3T3Q**, **3T3R**, **3T3S**, and **3T3Z**.

Enzymes: EC: 1.14.14.1

Introduction

The cytochrome P450 superfamily contains enzymes that catalyze oxidative metabolism of the myriad of lipophilic drugs and xenobiotics to which humans are exposed. Each different cytochrome P450 enzyme can bind, metabolize, and be inhibited by a distinctive set of chemically and structurally diverse compounds. However, a single compound can often interact with multiple P450 enzymes. Understanding the structural basis for this overlapping ligand selectivity is important in order to rationalize and predict the participation of various human cytochrome P450 enzymes in drug and xenobiotic metabolism, as well as their respective susceptibilities to inhibitors.

In humans, the CYP2A and CYP2E subfamilies represent an excellent system for such structure/function investigations. In humans, the functional CYP2A enzymes consist of two 94% identical enzymes: CYP2A6, which is largely hepatic [1], and CYP2A13, which is primarily located in the respiratory tract [2, 3]. Humans also have a single CYP2E1 enzyme, which is primarily hepatic [1] and has less than 40% amino acid identity compared to the CYP2A enzymes. Nonetheless, CYP2E1 oxidizes and is inhibited by many of the same compounds as CYP2A enzymes. For example, *p*-nitrophenol and chlorzoxazone have traditionally been used as substrates to indicate the presence of active CYP2E1 protein, especially in microsomes where mixtures of P450 enzymes are present, but CYP2A13 has a higher catalytic efficiency than CYP2E1 for both substrates [4]. In comparison, CYP2A6 has a lower catalytic efficiency for chlorzoxazone 6-hydroxylation and equivalent catalytic efficiency for *p*-nitrophenol 2-hydroxylation compared to CYP2E1 [4]. Styrene and toluene are also metabolized by CYP2E1, CYP2A13, and CYP2A6 [4].

Although there are various structures available of CYP2A6, CYP2A13, and CYP2E1, none of them offer a direct comparison because they all contain different ligands [5–9], and a single cytochrome P450 enzyme can often bind different ligands with different active site topologies. This appears to be especially true for CYP2E1, which is known to have dramatically different active site volume and topography depending on the ligand [5, 6]. To probe the differences and similarities between the human CYP2A and CYP2E1 enzymes, we utilized the muscarinic receptor agonist pilocarpine ((3*S*,4*R*)-3-ethyl-4-((1-methyl-1*H*-imidazol-5-yl)methyl)dihydrofuran-2(3*H*)-one, Figure 1). Pilocarpine was previously identified as a competitive inhibitor of human CYP2A6, and to a lesser extent CYP2B6 [10, 11]. We have determined herein that pilocarpine also inhibits CYP2A13 and CYP2E1.

In the present study functional analysis of CYP2A13, CYP2A6, and CYP2E1 with pilocarpine combined with X-ray structures of these complexes have allowed direct comparisons among these three different human cytochromes P450. In addition, wild type CYP2A13 and CYP2A6 were compared to a previously identified CYP2A6 mutant, CYP2A6 I208S/I300F/G301A/S369G, that gained the ability to metabolize phenacetin like CYP2A13 [12]. Previous studies suggested that these four residues were the primary determinants for CYP2A phenacetin metabolism and might be important for differential recognition of other ligands by CYP2A enzymes. The functional and structural results presented herein allow for a direct comparison of all three enzymes and provides insight to observed differences in inhibition by pilocarpine.

Results

Pilocarpine binding

Titrations of pilocarpine with CYP2A6, CYP2A6 I208S/I300F/G301A/S369G, and CYP2A13 result in increases in absorbance at 424 nm and decreases at 420 nm, consistent with a type II interaction in which a nitrogen coordinates to the heme iron (Figure 1A–C).

Titrations of CYP2E1 with pilocarpine were more unusual (Figure 1D). At low pilocarpine concentrations, absorption increases were observed at 391 nm and decreases at 430 nm, indicative of a type I interaction in which pilocarpine binding displaces of a water molecule from the heme iron but does not interact directly with the heme itself. However at higher pilocarpine concentrations, the type I shift disappeared and a type II shift was observed similar to the CYP2A enzymes. The dissociation constants for type II binding to all three CYP2A enzymes were very similar (1.5–3.6 μM, Figure 1A–C), while the same parameter for CYP2E1 was 10-fold higher (26.5 μM, Figure 1D).

Pilocarpine Inhibition

Pilocarpine inhibition constants were determined for CYP2A6, CYP2A6 I208S/I300F/G301A/S369G, CYP2A13, and CYP2E1 using both common and selective substrates (Table 1). Coumarin was used as the selective substrate for all of the CYP2A enzymes, while chlorzoxazone was used as an additional substrate for CYP2E1. Since CYP2E1, CYP2A13, and CYP2A6 all metabolize *p*-nitrophenol, pilocarpine inhibition was also evaluated for all three wild type enzymes with *p*-nitrophenol as the substrate. These results revealed that pilocarpine is a competitive inhibitor of CYP2A13 for both coumarin and *p*-nitrophenol, though the K_i is 34-fold higher for coumarin. CYP2A6 inhibition by pilocarpine revealed mixed inhibition, with K_i values for both substrates 2-fold higher than for CYP2A13. The CYP2A6 quadruple mutant I208S/I300F/G301A/S269G demonstrated competitive inhibition with a K_i for inhibition of coumarin 7′-hydroxylation nearly identical to that of wild type CYP2A13 with the same substrate. Pilocarpine inhibited CYP2E1 least effectively with non-competitive inhibition with both chlorzoxazone and *p*-nitrophenol as substrates. By comparison, pilocarpine had a K_i value for CYP2E1 546-fold greater than CYP2A13 with the same substrate.

Structure of CYP2A6 with pilocarpine

The protein backbone of CYP2A6 with pilocarpine is very similar to other structures of CYP2A6. The average root mean square deviations of the CYP2A6/pilocarpine structure with available structures of CYP2A6 with coumarin, methoxsalen, N,N-dimethyl(5-(pyridin-3- yl)furan-2-yl)methanamine, N-methyl(5-(pyridin-3-yl)furan-2-yl) methanamine, (5-(pyridin-3-yl)furan-2-yl)methanamine and adrithiol is 0.24 Å [8, 9]. In the present CYP2A6 structure, density for pilocarpine was located directly above the heme in all four CYP2A6 molecules. This density clearly oriented pilocarpine with the imidazole ring closest to the heme, with a distance of only 2.3 Å from the unsubstituted nitrogen in the imidazole ring to the heme iron (Figure 2A). This is consistent with the type II spectral shift observed in the spectral ligand-binding assay (Figure 1A). The furan ring packs against the I helix with a weak hydrogen bond from the exocyclic keto oxygen of pilocarpine to the N297 NH_2 donor (3.4 Å). The ethyl group of the furan ring is directed toward L370. Additional residues that pack against pilocarpine include F107, F209, V117, F118, I300, L370, and I366.

Structure of CYP2A13 with pilocarpine

The structure of CYP2A13 with pilocarpine has a protein backbone very similar to that of a structure of CYP2A13 with indole [7] (RMSD 0.53 Å). Due to the lower (3.0 Å) resolution, the density for pilocarpine was not as well defined in the CYP2A13 active site, but the ligand could be modeled with reasonable certainty in six of the eight molecules. The $2|F_o|-|F_c|$ map (Figure 2b, blue mesh) has one portion of the pilocarpine with poor coverage—the ethyl side chain—but its placement was determined based on the σ_A-weighted composite omit map (Figure 2B, pink mesh). Similar to the CYP2A6 structure, pilocarpine in the CYP2A13 active site is oriented with the imidazole ring closest to the heme with a distance of only 2.5 Å from the unsubstituted nitrogen to the heme iron. This is also consistent with

the type II spectral shift observed in the spectral ligand binding assay for this enzyme (Figure 1B). As in the case of CYP2A6, there appears to be a hydrogen bond from the furan ring keto oxygen to N297 (3.0 Å). The furan ring is in a similar overall placement as in CYP2A6 except for the ethyl side chain, which is directed in the opposite direction—toward F300 rather than toward L370. Residues F107, A117, F118, F209, F300, L370, and L366 all pack against pilocarpine in the CYP2A13 active site (Figure 2B).

Structure of CYP2A6 I208S/I300F/G301A/S369G with pilocarpine

The protein backbone of the CYP2A6 I208S/I300F/G301A/S369G mutant is very similar to that of the same mutant with the substrate phenacetin bound (RMSD 0.27 Å). This CYP2A6 I208S/I300F/G301A/S369G structure also contained four copies of CYP2A6 in the asymmetric unit and each copy contained density corresponding to pilocarpine clearly defined above the heme. Like the CYP2A13 and the CYP2A6 structures, the imidazole ring of pilocarpine is located close to the heme with the unsubstituted nitrogen 2.5 Å from the heme iron (Figure 2C) consistent with the type II spectral shift observed in the spectral ligand binding assay (Figure 1C). Although the plane of the furan ring is different in that it stacks with F107 instead of against the I-helix as in CYP2A6 and CYP2A13, the hydrogen bond from the keto oxygen on the furan ring to N297 (3.0 Å) is maintained. Additional residues that pack against the pilocarpine include F107, V117, F209, F300, A301, I366, and L370.

Structure of CYP2E1 with pilocarpine

The protein backbone of the CYP2E1 structure with pilocarpine is very similar to that of CYP2E1 with indazole, 4-methylprazole, and omega-imidazolyl fatty acid analogs [5, 6] with an average RMSD of 0.31 Å. Like the CYP2A structures, the density in this 2.35 Å structure supported the clear placement of pilocarpine with the imidazole ring ~2.18 Å from the heme iron (Figure 2D), consistent with the type II spectral shift observed at high pilocarpine concentrations (Figure 1D). In this orientation no hydrogen bond is observed between pilocarpine and active site residues. Despite the presence of D295 in CYP2E1 at the position corresponding to N297 in CYP2A enzymes, in CYP2E1 D295 is shielded from pilocarpine by I115 and, as a result, the CYP2E1 active site is much more hydrophobic. Instead, pilocarpine is surrounded by several hydrophobic residues including I115, L368, V364, and phenylalanines (F116, F106, F207, F298, and F478) with T303 as the only polar residue.

Discussion

Comparison of CYP2A6 and CYP2A13

There are many similarities between the functional and structural characteristics of CYP2A6 and CYP2A13. CYP2A6 and CYP2A13 bind pilocarpine with similar, single-digit micromolar affinities, and have only a two-fold difference in the K_i value with two different substrates. The overall structural similarity is very high (RMSD 0.63 Å). The structural and functional evidence agree that pilocarpine binds with an imidazole nitrogen directly coordinated to the heme iron (Figure 1A, B and Figure 3A). Additionally, both structures show the exocyclic oxygen of pilocarpine positioned within hydrogen bonding distance to the conserved N297, one of only two polar residues lining the active site. The primary difference in pilocarpine binding to these two wild type enzymes is in the orientation of the ethyl group of the furan ring (Figure 3A). In CYP2A13, this ethyl group is directed toward residue 300 and away from F118 and L370, while in CYP2A6 the ethyl group is oriented in the opposite direction, towards F118 and L370 and away from residue 300. Residue 300 is a phenylalanine in CYP2A13 and an isoleucine in CYP2A6, while F118 and L370 are conserved. Although there are eleven first and second shell amino acid differences between

the CYP2A6 and CYP2A13 active sites, the side chain present at position 300 may be one of the most significant differences between the two active sites. The identity of the residue at position 300 not only correlates with the ethyl orientation in pilocarpine in the CYP2A6 and CYP2A13 structures reported herein, but also with the ability to bind and monooxygenate phenacetin [12]. This is also a key residue in the binding of other ligands including 2′-methoxyacetophenone, phenethyl isothiocyanate, and coumarin [13]. In addition to the role for the nonconserved residue at position 300, there are also several differences in the orientation of the three conserved phenylalanine residues, F118, F107, and F209, which line the active site. Overall, the sizes of the two active sites are similar, with the CYP2A6 volume (281.7 $Å^3$) slightly smaller than of CYP2A13 (309.4 $Å^3$), but the proportions are different (Figure 3B). The CYP2A13 active site has more space available for ligands near F300 and F209 due to a combination of the phenylalanine at residue 300 and positioning of F209 away from the active site in the CYP2A13 structure, while the CYP2A6 active site has more volume available to the ligand near F118 and above L370 (Figure 3B).

Comparison of CYP2A6, CYP2A6 I208S/I300F/G301A/S369G, and CYP2A13

The CYP2A6 I208S/I300F/G301A/S369G quadruple mutant has a binding affinity for pilocarpine similar to that for both CYP2A wild type enzymes, but a K_i for pilocarpine that is essentially identical to CYP2A13 and thus 2-fold lower than CYP2A6 (Figure 1, Table 1). Based on both this information and the ability of this CYP2A6 quadruple mutant to bind and deethylate phenacetin like wild type CYP2A13 (as opposed to CYP2A6, which does not bind phenacetin [12]), we had proposed that the CYP2A6 I208S/I300F/G301A/S369G mutant might orient pilocarpine as observed in wild type CYP2A13 rather than as observed in CYP2A6.

Comparison of the three pilocarpine CYP2A structures (Figure 3C) revels that two key features are shared in all three structures: 1) the placement of the imidazole ring and direct coordination of the nitrogen to the heme iron, and 2) a conserved hydrogen bond from the keto oxygen on the furan ring to N297. In the CYP2A6 quadruple mutant, the ethyl side chain of pilocarpine is oriented towards residue 300 and away from residues F118 and L370, similar to the CYP2A13 wild type structure. Additionally, several residues are found in essentially identical positions as CYP2A13, including the mutated residues F300, A301, S208, and G369. However, despite maintaining a hydrogen bond to N297, the pilocarpine furan ring is oriented very differently in the CYP2A6 I208S/I300F/G301A/S369G structure (Figure 3C) compared to either the CYP2A6 or CYP2A13 structures. Instead of packing against the I helix, the furan ring rotates in CYP2A6 I208S/I300F/G301A/S369G so that the furan face is more parallel with F107. The two nearby residues that differ significantly in their positions between the CYP2A6 quadruple mutant and CYP2A13 are the conserved residues L370 and F118. In the CYP2A6 I208S/I300F/G301A/S369G mutant, the L370 side chain is deflected away from the central active site compared to its position in CYP2A13 or CYP2A6, allowing sufficient volume for the furan ring of pilocarpine to rotate in a different manner than observed in CYP2A13 or CYP2A6 (Figure 3C). Residue F118 is found in the same position in CYP2A6 I208S/I300F/G301A/S369G as the wild type CYP2A6, a position that also results in additional active site volume (Figure 3C). In addition, there is one amino acid in this region that differs between CYP2A13 and CYP2A6—residue 117, which is a valine in CYP2A6 and the CYP2A6 quadruple mutant, and an alanine in CYP2A13. This residue, in addition to the position of conserved residue L370, may play a role in the positioning of pilocarpine in the active site of CYP2A6 along with residues 208, 300, 301, and 369. Thus, although the CYP2A6 I208S/I300F/G301A/S369G mutant has nearly identical functional characteristics to CYP2A13 with both the substrate phenacetin and the inhibitor pilocarpine, it is not a complete structural mimic of the CYP2A13 active site for all ligands.

Comparison of the inhibitor pilocarpine in CYP2E1 vs. CYP2A enzymes

Functional evaluation indicates that CYP2E1 has a type II affinity for pilocarpine that is ~8-fold lower than the wild type CYP2A enzymes and has a 250- to 550-fold higher K_i (Figure 1, Table 1). Pilocarpine binding to CYP2E1 is unusual in that at low concentrations of pilocarpine, type I binding is observed, converting to type II binding at higher pilocarpine concentrations (Figure 1D). This suggests that pilocarpine may bind in more than one mode. In addition, inhibition assays with pilocarpine indicate that pilocarpine is a non-competitive inhibitor of CYP2E1. The non-competitive nature of the inhibitor suggested that pilocarpine might bind in a second mode or second location. There is evidence for a second binding site in the sigmoidal kinetics of several human xenobiotic cytochrome P450 enzymes and some structural evidence as well. Most notable is a crystal structure of CYP3A4 with the antifungal ketoconazole which identified two molecules of ketoconazole in the active site, one located close to the heme and the second located above the first [14]. The structure of CYP2C9 with warfarin also has evidence of a secondary binding site as warfarin is located too far from the heme for metabolism to occur [15]. However, the CYP2E1 structure with pilocarpine showed no evidence for pilocarpine binding anywhere other than immediately adjacent to the heme in the active site of CYP2E1. This is likely due to the very high concentration of pilocarpine (100 mM) present in the crystallization condition. The type I shift was only present at low concentration of pilocarpine (<10 μM).

CYP2A and the CYP2E1 enzymes have active sites that are primarily hydrophobic with a roof composed of phenylalanine residues. Several of the key hydrophobic residues in CYP2E1 have equivalents in the CYP2A enzymes (Figure 4A). For example, CYP2E1 has a leucine at residue 368 that is structurally equivalent to the leucine at 370 in CYP2A enzymes. There are also several structurally equivalent phenylalanine residues that result in a very differently shaped active site in CYP2E1 compared to the CYP2A enzymes (F207, F298, and F478 in CYP2E1 for the CYP2A F209, F300, and F480) (Figure 4A). At the position corresponding to the hydrogen bond donor N297, the CYP2E1 active site has D295, but it does not hydrogen bond with pilocarpine because I115 and F298 block the residue from actually forming part of the active site. Perhaps due in part to these differences, the pilocarpine orientation in the CYP2E1 active site is much more perpendicular to the heme than in the CYP2A enzymes where this axis is more parallel to the I helix (Figure 4A). The hydrogen bond interaction with N297 in CYP2A enzymes in addition to the imidazole ring interaction with the heme may account for the higher binding affinity and lower K_i values for pilocarpine in the CYP2A enzymes.

In the first shell of residues composing the CYP2E1 active site the absence an amino acid corresponding to CYP2A N297 that can participate in a ligand-stabilizing hydrogen bond may also explain why pilocarpine binding to CYP2E1 can display both type I and type II interactions. In addition to the orientation observed in the structure with imidazole interacting with the heme (type II), pilocarpine may also bind in a non-coordinating orientation (type I). Available active site space suggests that pilocarpine may also be able to bind so that the dihydrofuran ring orients toward the heme, with the exocyclic oxygen interacting with the only hydrophilic amino acid, T303.

Comparison of the CYP2E1 active site with structures containing other ligands

The volume of the CYP2E1 active site is ~190 $Å^3$ with the low MW ligands indazole or 4-methylpyrazole and 420–470 $Å^3$ with fatty acid substrate analogs of various chain lengths [5, 6] (Figure 4B). The active site volume of CYP2E1 with pilocarpine is 332.7 $Å^3$, a volume slightly larger than the active sites of CYP2A6 and CYP2A13 with pilocarpine (280 and 310 $Å^3$, respectively), and intermediate between the other reported CYP2E1 structures. However, the active site topology with pilocarpine is different yet again from the other two

types of 2E1 structures reported previously. Differences in the CYP2E1 active site dimensions with fatty acid vs. low MW ligands arose through rotation of the F298 side chain without a shift in the backbone [6]. The CYP2E1/pilocarpine backbone also overlays with both of the other types of CYP2E1 structures, but in this case rotation of the F478 side chain opens up the opposite wall of the active site to accommodate pilocarpine (Figure 4B).

The current set of structural and functional data allows for a detailed comparison of binding of the same ligand across human cytochrome P450 subfamilies 2A and 2E. In the current series, pilocarpine binding is different for both the CYP2A6 and CYP2A13 enzymes, as well as for CYP2E1, and those disparities can be correlated to detailed differences in the respective active sites. Overall, the binding of pilocarpine into the active site of CYP2A enzymes appears to be driven primarily by hydrogen bonding with the conserved N297 and steric interactions largely driven by both a small set of nonconserved residues (300, 301, 208, 369 and perhaps 117) and indirect effects of a few conserved residues such as L370 and F209. In other words, the pilocarpine ligand largely adapts its conformation to fit into the CYP2A active sites. Remarkably, the CYP2E1 active site appears to bind ligands in an entirely different manner. The binding of pilocarpine induces yet a third distinct conformation of the CYP2E1 active site, generated by changes in side chain conformations. In other words, CYP2E1 demonstrates much larger variation in the active site topology to accommodate various ligands. To date, none of the liganded structures of CYP2A enzymes indicate this same type of flexibility. It remains to be seen if structures of CYP2A enzymes with other ligands will reveal active sites that have essentially the same topology as those already known, or if additional data points will reveal more diversity in the CYP2A active site dimensions. This is especially true for CYP2A13 since only two structures have been reported to date, including the one presented herein. If the CYP2A structures are much less flexible than those observed for CYP2E1 and other xenobiotic cytochrome P450 enzymes, this has positive implications for the accuracy of docking to predict drug metabolism and procarcinogen bioactivation by these human CYP2A enzymes.

Experimental Procedures

Protein Design, Expression, and Purification

Truncated, His-tagged but fully functional versions of human CYP2A6, CYP2A6 I208S/G301A/I300F/S369G, CYP2A13, and CYP2E1 proteins were designed, expressed, and purified as described previously [5, 12].

Spectral Binding Assay

Ligand binding affinities were determined using a spectral ligand binding assay described previously [13].

Enzyme Assay

All metabolism and inhibition assays used a reconstituted protein system (RPS) consisting of 50 pmol of purified CYP2A or CYP2E1 protein incubated with 200 pmol NADPH-cytochrome P450 reductase and 100 pmol cytochrome b_5 in a 1:4:2 ratio for 20 minutes at room temperature prior to use. This RPS mixture was added to assay buffer containing the desired substrate and inhibitor. The samples were pre-incubated at 37° C for 3 minutes and the reactions were initiated by the addition of 1 mM NADPH. Samples were incubated for 10 minutes at 37° C and the reaction was stopped with 300 μL of 20% trichloroacetic (TCA) on ice. All standards and zero samples had 300 μL of 20% TCA added prior to the addition of NADPH. Samples and standards were centrifuged at 4500 × g for 10 minutes.

Coumarin 7-hydroxylation

RPS was added to buffer (50 mM Tris, pH 7.4 and 5 mM $MgCl_2$) containing coumarin and pilocarpine. After completing the assay as described above, all samples and standards were diluted by the addition of 1 mL (2A6) or 200 μL (2A13) of buffer (50 mM Tris, pH 7.4 and 5 mM $MgCl_2$). The amount of 7-hydroxycoumarin present was determined by fluorescence following HPLC separation. The 7-hydroxycoumarin metabolite was detected by fluorescence with an excitation wavelength of 355 nm and emission wavelength of 460 nm. The mobile phase consisted of 30% MeOH, 68% water, and 2% acetic acid with a 1 mL/min flow rate and a sample volume of 10 μL.

para-Nitrophenol (PNP) 4-hydroxylation

RPS was added to 100 mM potassium phosphate pH 6.8 with 2 mM ascorbic acid (for CYP2E1), *p*-nitrophenol, and pilocarpine. After assay completion as described above, the amount of 4-nitrocatechol was determined following HPLC separation. A mobile phase of 27% acetonitrile and 0.2% acetic acid was run at a rate of 1 mL/min. Monitoring absorption at 345 nm allowed the detection of 4-nitrocatechol at ~5 minutes with *p*-nitrophenol elution at ~8 minutes.

Chlorzoxazone 6-hydroxylation

The RPS was added to 100 mM potassium phosphate buffer, pH 7.4 and varying concentrations of chlorzoxazone and pilocarpine. Instead of trichloroacetic, sample reactions were stopped after 10 minutes at 37° C by the addition of 25 μL of 60% perchloric acid. Correspondingly standards and controls had 25 μL of 60% perchloric acid, instead of trichloroacetic, added prior to the addition of NADPH. The 6-hydroxychlorzoxazone metabolite was detected using an absorption wavelength of 287 nm on an HPLC with a mobile phase consisting of 20% acetonitrile, 78% water, and 2% acetic acid with a 1 mL/min flow rate.

Protein Crystallization, Data Collection, and Structure Determination

CYP2A6, CYP2A6 I208S/I300F/G301A/S369G, CYP2A13, and CYP2E1 were co-crystallized with pilocarpine by hanging drop vapor diffusion. The CYP2A6/pilocarpine crystals were grown from 500 μM CYP2A6 with 100 mM pilocarpine in CM elution buffer (50 mM potassium phosphate buffer, pH 7.4, 20% glycerol, 1 mM EDTA, 0.5 M NaCl) with 2% Anapoe-35 in a 1:1 ratio with precipitant solution (30% PEG 3500, 0.175 M Tris, pH 8.5, and 0.2 M ammonium sulfate). The CYP2A6 quadruple mutant/pilocarpine crystal was grown similarly using 100 μM CYP2A6 I208S/I300F/G301A/S369G protein with 100 mM pilocarpine in CM elution buffer and 2% Anapoe-35 in a 1:1 ratio with a slightly modified precipitant solution (30% PEG 3350, 0.100 M Tris, pH 8.5, and 0.200 M ammonium sulfate). The CYP2A13/pilocarpine crystal was grown from a solution of 200 μM CYP2A13, 100 mM pilocarpine, and 2% Anapoe-35 in CM elution buffer in a 2:1 ratio with precipitant solution (30% PEG 3350, 0.175 M Tris, pH 8.5, and 0.2 M ammonium sulfate). The CYP2E1 crystal was grown at 455 μM in a buffer containing 100 mM pilocarpine, 120 mM potassium phosphate, pH 7.4, 0.5 M sucrose, and 1 mM EDTA in a 1:1 ratio with precipitant solution (8% PEG MME 2000, 12% isopropanol, and 0.1 M NaHEPES, pH 7.5).

Crystals were flash cooled in liquid nitrogen after being immersed in a cryoprotectant. For all CYP2A crystals, the cryoprotectant consisted of 700 μL of synthetic mother liquor and 300 μL of 100% ethylene glycol. The cryoprotectant for CYP2E1 was 0.1 M NaHEPES, pH 7.5, 5% iso-propanol, and 1.4 M sucrose. X-ray diffraction data of CYP2A6, CYP2A6 I208S/I300F/G301A/S369G, and CYP2A13 each with pilocarpine were collected at the Stanford Synchrotron Radiation Laboratory (Stanford, CA) on Beamline 9–2 using a 0.98 Å

wavelength and temperature of 100 K. Data were processed using Mosflm and Scala [16, 17]. The CYP2E1/pilocarpine data set was collected on Beamline 17-BM at the Advanced Photon Source and processed with HKL2000. All structures were solved by molecular replacement with the program Phaser [17]. Model building and refinement of all structures were done iteratively using COOT [18] and Refmac5 in the CCP4 suite [17]. Detailed collection and refinement statistics are presented in Table 2.

The search model for CYP2A13 with pilocarpine was a 1.65 Å structure of CYP2A6 with N-methyl(5-(pyridin-3-yl)furan-2-yl)methanamine (**PDB 2FDV**). A Matthew's coefficient of 2.88 with 57.4% solvent suggested 8 molecules in the asymmetric unit. Molecular replacement identified 8 molecules in CYP2A13 with good packing. The 3.0 Å final model of 2A13 with pilocarpine contains residues 32–494 in molecules A–H, heme, 6 pilocarpine molecules, and 31 water molecules and is deposited in the PDB as **3T3S**. The crystallographic R-factor is 21.3% and the R_{free} is 30.3%. In the Ramachandran plot, 86.2% of the residues are in the most favored region, 13.0% in the additionally allowed, 0.5% in the generously allowed, and 0.3% in the disallowed regions.

The search model for both CYP2A6 structures was a 1.9 Å structure of CYP2A6 complexed with coumarin (**PDB 1Z10**, molecule B). The 2.4 Å structure of CYP2A6 with pilocarpine contains residues 32–494 and heme in all four copies of the asymmetric unit, 4 pilocarpine molecules, and 217 water molecules and is deposited in the PDB as **3T3R**. The crystallographic R-factor is 19.9% and the R_{free} is 26.0%. In the Ramachandran plot, 91.5% of the residues are in the most favored region, 8.2% in the additionally allowed, 0.4% in the generously allowed, and 0.2% in the disallowed regions.

The 2.1 Å final model for 2A6 I208S/I300F/G301A/S369G with pilocarpine contains residues 32–494 and heme in all four molecules, 4 pilocarpine molecules, and 504 water molecules and is deposite in the PDB as **3T3Q**. The crystallographic R-factor is 21.2% and the R_{free} is 25.7%. In the Ramachandran plot 91.2% of the residues are in the most favored region, 8.1% in the additionally allowed, 0.3% in the generously allowed, and 0.2% in the disallowed regions.

The 2.35 Å final model of CYP2E1 with pilocarpine contains residues 31–494, heme, and pilocarpine in all four molecules. There were also 4 sucrose molecules and 772 water molecules and is deposited in the PDB as **3T3Z**. The crystallographic R-factor is 21.7% and R_{free} is 28.1%. In the Ramachandran plot 89.6% of the residues were in the most favored region, 9.9% in additionally allowed, 0.2% in generously allowed, and 0.2% in the disallowed regions.

In each structure the single residue found in the disallowed region of the Ramachandran plot was well defined by electron density.

Protein Figures and Analysis

All protein figures were generated using PyMOL [19]. VOIDOO [20] was used to determine active site volumes with a 1.4 Å probe size. All figures were made using molecule A for CYP2A6, CYP2A6 I208S/I300F/G301A/S369G, and CYP2E1. All figures of CYP2A13 utilized molecule E as this molecule contained the best ligand density.

Acknowledgments

This work was supported, in whole or in part, by National Institutes of Health Grant GM076343 (EES). Crystals were grown using the facilities of the Protein Structure Laboratory at the University of Kansas supported by the National Institutes of Health Grant RR017708. The CYP2E1 data was collected at the Advanced Photon Source. Use of the IMCA-CAT beamline 17-BM at the Advanced Photon Source was supported by the companies of the

Industrial Macromolecular Crystallography Association through a contract with Hauptman-Woodward Medical Research Institute. Use of the Advanced Photon Source was supported by the U.S. Department of Energy, Office of Science, Office of Basic Energy Sciences, under Contract No. DE-AC01-06CH11357. The remainder of the X-ray data collection was carried out at the Stanford Synchrotron Radiation Laboratory, a national user facility operated by Stanford University on behalf of the United States Department of Energy Office of Basic Energy Sciences. The Stanford Synchrotron Radiation Laboratory Structural Molecular Biology Program is supported by the Department of Energy Office of Biological and Environmental Research, the National Institutes of Health National Center for Research Resources Biomedical Technology Program, and the National Institute of General Medical Sciences.

References

1. Bieche I, Narjoz C, Asselah T, Vacher S, Marcellin P, Lidereau R, Beaune P, de Waziers I. Reverse transcriptase-PCR quantification of mRNA levels from cytochrome (CYP)1, CYP2 and CYP3 families in 22 different human tissues. Pharmacogenetics and Genomics. 2007; 17:731–742. [PubMed: 17700362]
2. Su T, Bao ZP, Zhang QY, Smith TJ, Hong JY, Ding XX. Human cytochrome p450 CYP2A13: Predominant expression in the respiratory tract and its high efficiency metabolic activation of a tobacco-specific carcinogen, 4-(methylnitrosamino)-1-(3-pyridyl)-1-butanone. Cancer Res. 2000; 60:5074–5079. [PubMed: 11016631]
3. Zhu LR, Thomas PE, Lu G, Reuhl KR, Yang GY, Wang LD, Wang SL, Yang CS, He XY, Hong JY. CYP2A13 in human respiratory tissues and lung cancers: an immunohistochemical study with a new peptide-specific antibody. Drug Metab Dispos. 2006; 34:1672–1676. [PubMed: 16815959]
4. Fukami T, Katoh M, Yamazaki H, Yokoi T, Nakajima M. Human Cytochrome P450 2A13 Efficiently Metabolizes Chemicals in Air Pollutants: Naphthalene, Styrene, and Toluene. Chem Res Toxicol. 2008; 21:720–725. [PubMed: 18266326]
5. Porubsky PR, Meneely KM, Scott EE. Structures of human cytochrome P-450 2E1. Insights into the binding of inhibitors and both small molecular weight and fatty acid substrates. J Biol Chem. 2008; 283:33698–33707. [PubMed: 18818195]
6. Porubsky PR, Battaile KP, Scott EE. Human cytochrome P450 2E1 structures with fatty acid analogs reveal a previously unobserved binding mode. J Biol Chem. 285:22282–22290. [PubMed: 20463018]
7. Smith BD, Sanders JL, Porubsky PR, Lushington GH, Stout CD, Scott EE. Structure of the human lung cytochrome P450 2A13. J Biol Chem. 2007; 282:17306–17313. [PubMed: 17428784]
8. Yano JK, Hsu MH, Griffin KJ, Stout CD, Johnson EF. Structures of human microsomal cytochrome P450 2A6 complexed with coumarin and methoxsalen. Nat Struct Mol Biol. 2005; 12:822–823. [PubMed: 16086027]
9. Yano JK, Denton TT, Cerny MA, Zhang X, Johnson EF, Cashman JR. Synthetic inhibitors of cytochrome P-450 2A6: inhibitory activity, difference spectra, mechanism of inhibition, and protein cocrystallization. J Med Chem. 2006; 49:6987–7001. [PubMed: 17125252]
10. Kimonen T, Juvonen RO, Alhava E, Pasanen M. The inhibition of CYP enzymes in mouse and human liver by pilocarpine. Br J Pharmacol. 1995; 114:832–836. [PubMed: 7773543]
11. Kinonen T, Pasanen M, Gynther J, Poso A, Jarvinen T, Alhava E, Juvonen RO. Competitive inhibition of coumarin 7-hydroxylation by pilocarpine and its interaction with mouse CYP 2A5 and human CYP 2A6. Br J Pharmacol. 1995; 116:2625–2630. [PubMed: 8590980]
12. DeVore NM, Smith BD, Urban MJ, Scott EE. Key Residues Controlling Phenacetin Metabolism by Human Cytochrome P450 2A Enzymes. Drug Metab Dispos. 2008; 36:2582–2590. [PubMed: 18779312]
13. DeVore NM, Smith BD, Wang JL, Lushington GH, Scott EE. Key residues controlling binding of diverse ligands to human cytochrome P450 2A enzymes. Drug Metab Dispos. 2009; 37:1319–1327. [PubMed: 19251817]
14. Ekroos M, Sjogren T. Structural basis for ligand promiscuity in cytochrome P450 3A4. Proc Natl Acad Sci U S A. 2006; 103:13682–13687. [PubMed: 16954191]
15. Williams PA, Cosme J, Ward A, Angove HC, Matak Vinkovic D, Jhoti H. Crystal structure of human cytochrome P450 2C9 with bound warfarin. Nature. 2003; 424:464–468. [PubMed: 12861225]

16. Leslie AG. The integration of macromolecular diffraction data. Acta Crystallogr D Biol Crystallogr. 2005; 62:48–57. [PubMed: 16369093]
17. Evans P. The CCP4 suite: programs for protein crystallography. Acta Crystallogr D Biol Crystallogr. 1994; 50:760–763. [PubMed: 15299374]
18. Emsley, PaKC. Coot: model-building tools for molecular graphics. Acta Crystallogr D Biol Crystallogr. 2004; 60:2126–2132. [PubMed: 15572765]
19. DeLano, WL. The PyMOL Molecular Graphics System. DeLano Scientific; Palo Alto, CA: 2002.
20. Kleywegt, GJ.; Zou, JY.; Kjeldgaard, M.; Jones, TA. Chapter 17.1. In: Rossman, MG.; Arnold, E., editors. International Tables for Crystallography. Vol. F. Kluwer Academic Publishers; The Netherlands: 2001. p. 353-356.p. 366-367.

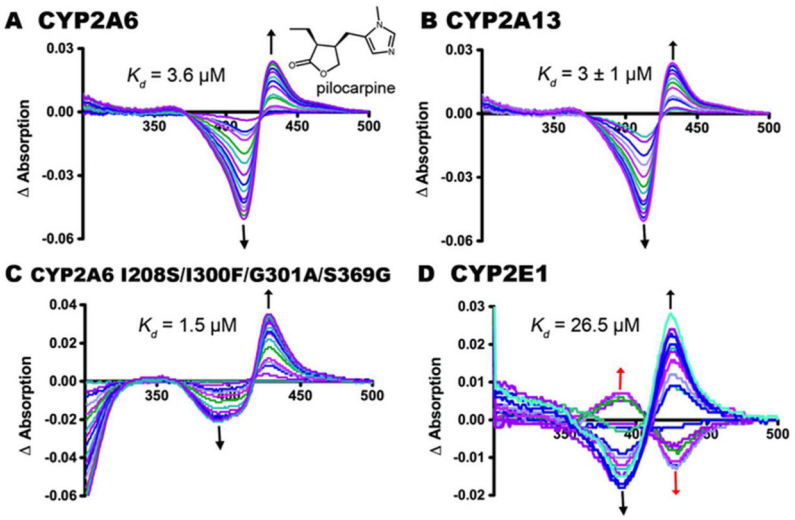

Figure 1.

Difference spectra upon titration of cytochrome P450 enzymes with pilocarpine and the resulting binding constants. Black arrows indicate the direction of type II shifts. (A) CYP2A6. (B) CYP2A13. (C) CYP2A6 I208S/I300F/G301A/S369G. (D) CYP2E1. Inset in panel A is the structure of pilocarpine. In this last panel, the red arrows indicate the type I spectral shifts that occur at lower concentrations of pilocarpine and black arrows indicate the type II shifts observed at higher pilocarpine concentrations. K_d values are the average of duplicate titrations, except for CYP2A13 where three titrations were performed.

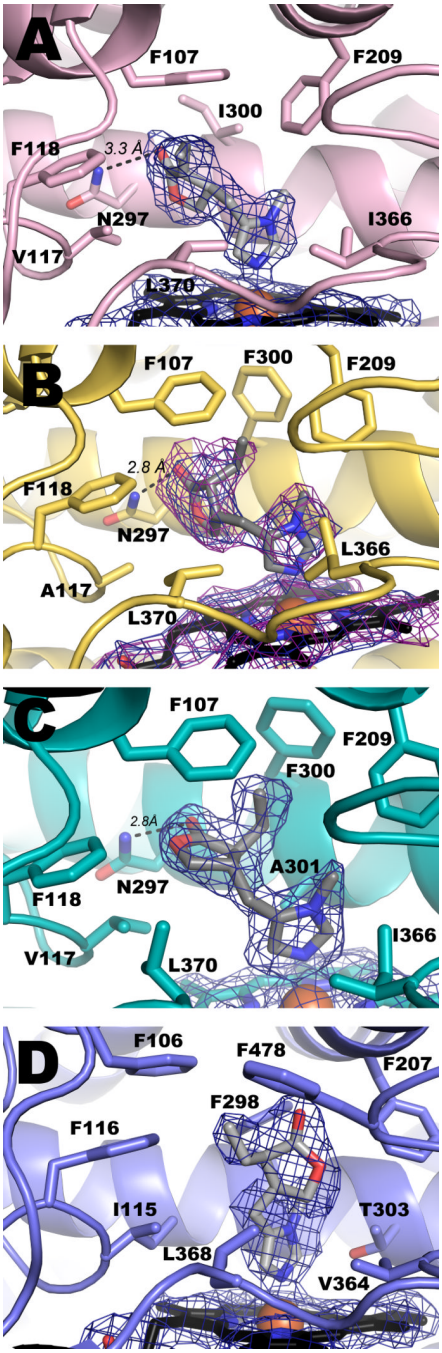

Figure 2.

Pilocarpine binding in the active site of CYP2A enzymes. CYP2A6 in pink (A), CYP2A13 in yellow (B), and CYP2A6 I208S/I300F/G301A/S369G in green (C) and CYP2E1 in indigo (D). In each panel the 2|Fo|-|Fc| electron density is 1.0 σ around the ligand and heme (blue mesh). In 2B, the σ_A-weighted composite omit map is also shown in pink mesh.

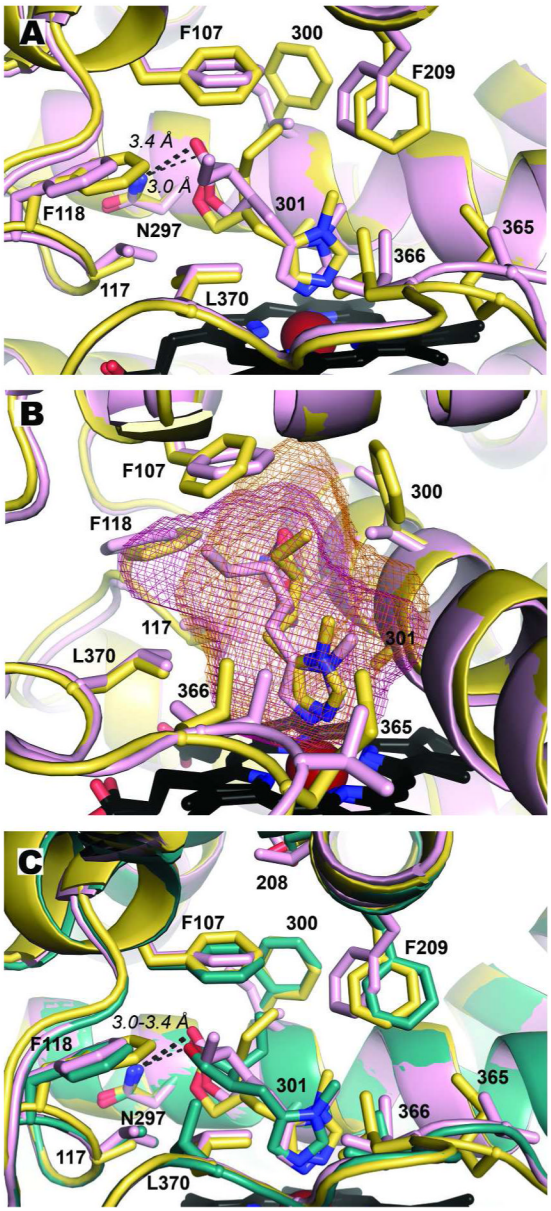

Figure 3.

Structural comparisons of CYP2A enzymes. Heme is shown as black sticks and iron as a red sphere. (A) Pilocarpine binds similarly in the CYP2A13 (yellow) and CYP2A6 (pink) active sites with the imidazole nitrogen coordinated to the heme iron and the furan exocyclic oxygen hydrogen bonded to N297. (B) CYP2A13 and CYP2A6 active sites (colored as panel A) with corresponding mesh illustrating the cavity volumes. Increased active site volume is available near residue 300 in CYP2A13 and near F118 in CYP2A6. (C) Comparison of CYP2A13 and CYP2A6 active sites (colored as in panel A) with the CYP2A6 I208S/I300F/G301A/S369G mutant (green). Although the imidazole ring/Fe interaction and hydrogen bond to N297 are conserved, the furan ring of pilocarpine is positioned differently in the CYP2A6 I208S/I300F/G301A/S369G mutant.

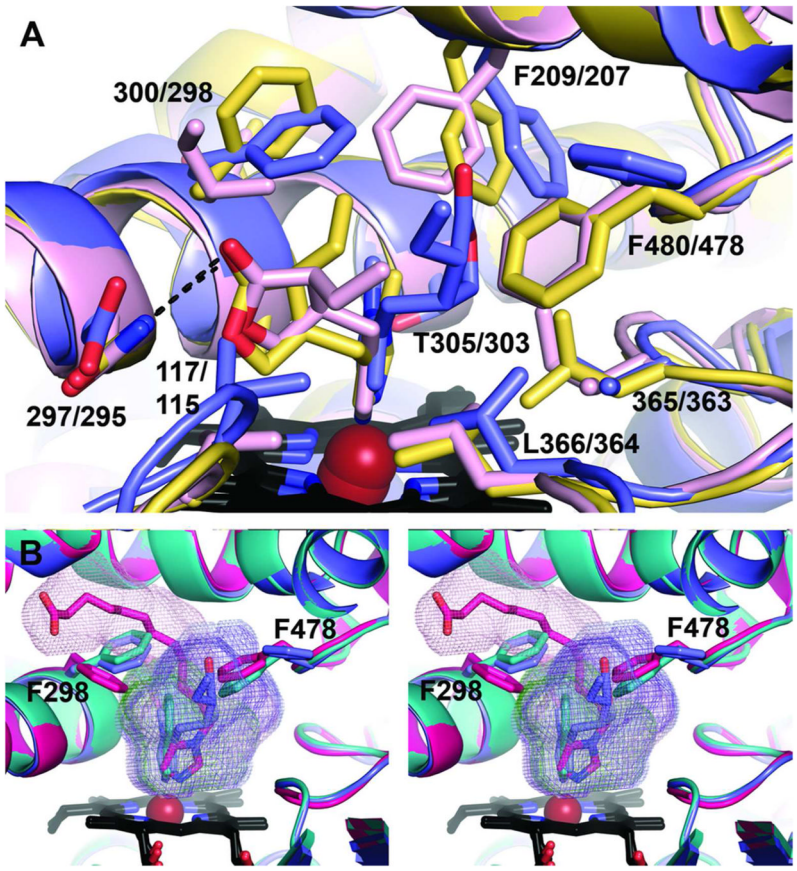

Figure 4.

Comparison of CYP2E1/pilocarpine complex to CYP2A structures with pilocarpine and to CYP2E1 structures with other ligands. Heme is shown as black sticks with iron as a red sphere. (A) The active sites of CYP2E1 (blue), CY2A6 (pink), and CYP2A13 (yellow) are similar in that all three contain several hydrophobic residues, including key phenylalanines which form the top of the active site (numbering is CYP2A/CYP2E1). (B) Comparison of CYP2E1 showing the active site voids (as mesh) for three different ligands: pilocarpine (blue), indazole (**PDB 3E6I**, cyan), and omega-imidazolyl-dodecanoic acid (**PDB 3LC4**, magenta). Changes in the active site topology are largely due to reorientation of either the F478 or F298 side chains with little alteration of the overall protein backbone. Figure is presented as a wall-eyed stereo figure.

Table 1

Inhibition constants for pilocarpine to CYP2A6, CYP2A6 I208S/I300F/G301A/S369G, CYP2A13, and CYP2E1

Enzyme	Substrate	Type of Inhibition	K_i (μM)[a]	K_i/K_i2A13[b]
CYP2A13	Coumarin	Competitive	48 ± 4	1
	p-Nitrophenol	Competitive	1.4 ± 0.1	1
CYP2A6	Coumarin	Mixed, α=6.98[c]	101± 17	2.1
	p-Nitrophenol	Mixed, α=24.9 [c]	3.0 ± 0.5	2.1
CYP2A6 I208S/I300F/G301A/S369G	Coumarin	Competitive	49 ± 3	1
CYP2E1	Chlorzoxazone	Non-competitive	360 ± 30	
	p-Nitrophenol	Non-competitive	765 ± 30	546

[a] All assays were preformed in triplicate.

[b] Fold difference between indicated K_i and the K_i for CYP2A13 with the corresponding substrate.

[c] Mixed inhibition with the larger alpha favors competitive inhibition, while the smaller alpha indicates more uncompetitive character to the inhibition.

Table 2

Crystal data collection and refinement statistics of cytochrome P450 enzymes binding pilocarpine.

	2A6	2A6 I208S/I300F/G301A/S369G	2A13	2E1
Crystal Data				
Space group	$P2_1$	$P2_1$	P1	P4
Unit cell				
a, b, c (Å)	70.34, 158.00, 104.45	70.95, 159.8, 103.9	71.50, 119.86, 154.87	100.6, 100.6, 259.5
α, β, γ(°)	90.0, 92.1, 90.0	90.0, 91.8, 90.0	101.0, 101.7, 93.6	90.0, 90.0, 90.0
Molecules per AU	4	4	8	4
Data Collection				
Resolution (Å)	87.04–2.40 (2.46-2.40)	87.04-2.10 (2.16-2.10)	117.00 - 3.00 (3.16-3.00)	37.0-2.35 (2.41-2.35)
Total observations[a]	237,442 (17,456)	301,406 (21,586)	383,997 (55,808)	385,690 (18,326)
Unique observations[a]	85,624 (6,420)	126,622 (9,537)	96,716 (14,053)	102,444 (10,635)
Completeness[a] (%)	96.5 (97.9)	94.3 (96.0)	98.3 (97.9)	95.9 (84.3)
Multiplicity[a]	2.8 (2.7)	2.4 (2.3)	4.0 (4.0)	3.76 (2.04)
R_{merge}[a] (%)	0.075 (0.400)	0.075 (0.400)	0.117 (0.634)	0.105 (0.221)
I/σI[a]	13.2 (3.4)	9.3 (1.4)	9.4 (2.1)	6.6 (2.6)
Refinement Statistics				
Resolution (Å)	79.00 – 2.40	63.32 – 2.10	102.88 – 3.00	36.98-2.35
No. reflections	81,313	120,218	91,882	97,337
R/R_{free} (%)	19.9/26.0	21.1/25.7	21.3/30.3	21.7/28.1
Rms bond lengths (Å)	0.020	0.009	0.017	0.020
Rms bond angles (°)	1.847	1.182	1.786	1.629
Number of atoms/Average B factor				
Protein	15,040/31.8	15,101/31.5	30,058/55.4	15,166/35.4
Ligand	60/34.0	60/39.1	90/72.8	60/26.7
Heme	172/20.2	172/21.3	344/52.2	172/22.1
Sucrose	0	0	0	92/28.8
Water	217/25.9	504/31.8	31/34.5	772/29.6
Coordinate error, Luzzati plot (Å)	0.277	0.254	0.388	0.321

[a]Parenthesis indicate highest resolution shell.